Title

Identification of Four Amoebicidal Nontoxic Compounds by a Molecular Docking Screen of Naegleria fowleri Sterol Δ8−Δ7-Isomerase and Phenotypic Assays

Journal

ACS Infectious Diseases, 5(12)

ISSN

2373-8227

Authors

Shi, Da
Chahal, Kirti Kandhwal
Oto, Patricia
et al.

Publication Date

2019-12-13

DOI

10.1021/acsinfecdis.9b00227

Peer reviewed

Published in final edited form as:

ACS Infect Dis. 2019 December 13; 5(12): 2029–2038. doi:10.1021/acsinfecdis.9b00227.

Identification of four amoebicidal non-toxic compounds by a molecular docking screen of *Naegleria fowleri* sterol Δ8−Δ7-isomerase and phenotypic assays

Da Shi[1,#], **Kirti Kandhwal Chahal**[1,2,#], **Patricia Oto**[1,#], **Louis-Felix Nothias**[1], **Anjan Debnath**[1], **James H. McKerrow**[1], **Larissa M. Podust**[1], **Ruben Abagyan**[1,*]

[1]Skaggs School of Pharmacy and Pharmaceutical Science, University of California San Diego,9500 Gilman Drive, La Jolla, California, 92093, United States of America

[2]Department of Pharmaceutical Sciences, Guru Jambheshwar University of Science and Technology, Hisar-Delhi Bypass Road, Hisar, Haryana 125001, India

Abstract

Naegleria fowleri is a free-living amoeba causing primary amoebic meningoencephalitis, a rapid-onset brain infection in humans with over 97% mortality rate. Despite some progress in the treatment of the disease, there is no single, proven, evidence-based treatment with a high probability of cure. Here we report the chemical library screening and experimental identification of four new compounds with amoebicidal effects against *N. fowleri*. The chemical library was screened by molecular docking against a homology model of sterol Δ8−Δ7 isomerase (NfERG2). Thirty top-ranking hits were then tested in a cell-based assay for anti-proliferative/amoebicidal activities. Eight chemicals exhibited nearly 100% inhibition of *N. fowleri* at 50 μM, with the EC_{50} values ranging from 6 μM to 25 μM. A cell toxicity assay using human HEK-293 cells was also performed. Four of the compounds preferentially kill amoeba cells with no apparent human cell toxicities. These compounds fall into two distinct chemical scaffolds with drug-like properties.

Graphical Abstract

*Corresponding author: ruben@ucsd.edu.
#These authors contributed equally

Conflicts of Interest

No potential conflict of interest was reported by the authors.

Supporting information

Supporting information containing LC-MS spectra of identified compounds, structural details of the 3D model and protein-ligand interactions, and details of cell-viability assay (20 figures), is available on the ACS publication website.

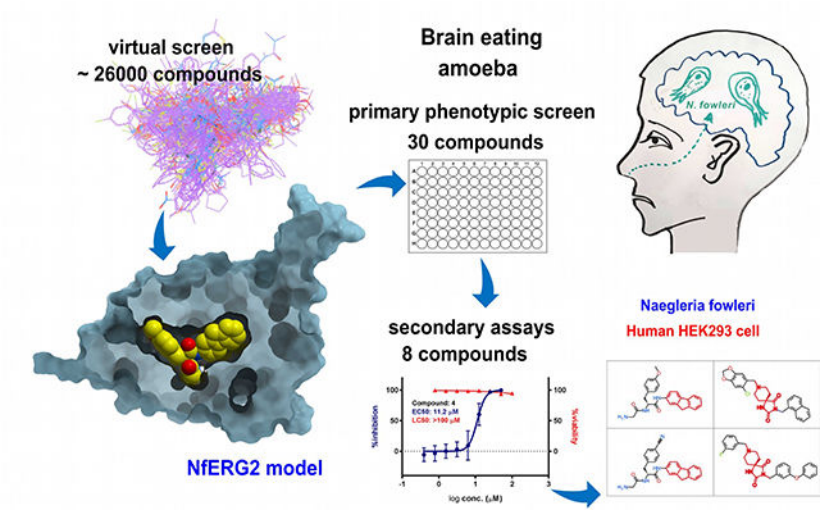

Keywords

drug discovery; homology modeling; *Naegleria fowleri*; primary amoebic meningoencephalitis; virtual ligand screen

Primary amoebic meningoencephalitis (PAM) is a rare but deadly disease caused by the opportunistic pathogen, *Naegleria fowleri*. *N. fowleri* is a free-living amoeba found in warm freshwater and soil habitats in all continents, except Antarctica[1–5]. *N. fowleri* mostly feeds on bacteria but after infecting humans it switches to human brain cells and causes severe brain inflammation and irreversible brain damage, leading to death [6–8].

Since the first report of PAM in 1965 in Australia, several hundred PAM cases have been reported worldwide. PAM is considered rare in the US with less than 10 reported cases per year [9]. However, this number is likely to be underestimated, because of diagnostic limitations and fast disease progression. Symptoms begin 1–9 days after the infection and disease results in nearly 97% mortality within the following two weeks [9].

High mortality associated with PAM results from the rapid onset, delayed diagnosis and lack of effective treatment. Until 2018, only 4 people in the U.S. out of 145 well documented cases had survived infection [10–12]. All survivors were treated with anti-fungal drug amphotericin B (AmpB), rifampicin, dexamethasone and one or more drugs from the following list: miconazole [12], fluconazole, miltefosine, and azithromycin [10–11]. No treatment regimen with consistent survival outcome has been established so far.

AmpB is used for serious fungal infections and leishmaniasis [13]. It acts through binding to ergosterol in the pathogen cell membranes, causing rapid leakage of monovalent ions, such as K^+ and Na^+ [14]. Other anti-fungal drugs, e.g. fluconazole and miconazole, act by inhibiting the sterol 14-demethylase (CYP51) and disrupting the ergosterol biosynthetic pathway [15]. Fluconazole, and some other “conazole” drugs (posaconazole, ketoconazole, voriconazole and itraconazole) were reported to kill *N. fowleri* in *in vitro* assays [16–18].

Drug discovery for PAM has been hindered by the lack of validated molecular targets and drug candidates that readily cross the blood-brain barrier (BBB). BBB permeability of drugs is a prerequisite for the treatment of brain infections. For example, only a small amount (~ 3% as compared to plasma concentration) of AmpB crosses the BBB [19], which may explain its limited efficacy against PAM. This limitation motivated us to look for new therapeutic targets and their inhibitors with strong amoebicidal activities and BBB permeability.

The sterol biosynthesis pathway has pathogen-specific enzymes in fungi and some protozoa, such as kinetoplastids and free-living amoeba [18, 20–22]. Successful development of the "conazole" group of antifungal drugs (miconazole, ketoconazole, voriconazole, etc.) demonstrated the feasibility of targeting this pathway[17, 23]. Furthermore, *N. fowleri* CYP51 and two other enzymes in this pathway, 24-sterol methyl transferase (24-SMT) and sterol Δ8−Δ7 isomerase (yeast ERG2 equivalent referred here as NfERG2), are validated as potentially druggable targets for anti-PAM drug development [16, 18].

Due to notable sequence similarity between the catalytic domain of ERG2 and human σ_1 non-opioid brain receptor, ERG2 is of particular interest for PAM drug discovery. NfERG2 catalyzes sterol Δ^8-Δ^7 double-bond isomerization in the pathway for biosynthesis of ergosterol, an essential component of *N. fowleri* plasma membranes (Fig. 1). Inhibition of NfERG2 depletes the intracellular ergosterol pool, disrupts cell and organelle membranes and induces autophagocytosis leading to *N. fowleri* death [18].

In this work, we applied a structure-based docking screen against a homology model of NfERG2 (AmoebaDB NF0056720), followed by experimental validation of hits in cell-based assays. First, based on the x-ray structure of human receptor (PDB ID: 5HK1) [24], we built a homology model of NfERG2 and identified a potentially druggable pocket using a pocket finding algorithm [25]. Then virtual ligand screening was performed by docking a library of 26,000 small molecules to the predicted pocket. Based on the *in silico* screening results, we tested 30 top ranking hits in a cell-based assay for efficacy against *N. fowleri* trophozoites. Out of eight experimentally active compounds, four compounds had high amoebicidal potencies and low human cell toxicity.

Results and Discussion

Homology modeling of ERG2 of *N. fowleri*

Given that no experimental ERG2 structure is yet available, we built a homology model of NfERG2 based on the crystal structure of the human σ1 non-opioid receptor (PDB ID 5HK1) [24]. The human σ1 receptor is implicated in various CNS diseases such as addiction, amnesia, pain and depression [26]. However, despite homology to ERG2, human σ1 receptor lacks Δ^8-Δ^7 isomerase activity [27]. Fig. 2a shows sequence alignment of the catalytic domain of NfERG2 and human σ1 receptor sharing 30% sequence identity and 60% sequence similarity over 177-amino acids length, which implies statistically significant structural similarity. Furthermore, it is known that the yeast ERG2 and mammalian σ1 receptor can be targeted with the same compounds. Thus, Moebius and co-authors tested 11 chemicals against the σ1 non-opioid receptor of guinea-pig and ERG2 of yeast, and found 10 chemicals out of 11 tested had similar binding affinities in both proteins [28–29]. To study the

conservation and relative importance of each position in ERG2, 369 sequences from different organisms, annotated in UniProt database as sterol Δ^8-Δ^7 isomerases, were aligned. The alignment conservation profile was added to the pairwise alignment of NfERG2 and human σ1 receptor (Fig. 2a).

The homology model was constructed using the computational tools implemented in ICM-Pro v3.8–6a software suite [30]. The structure of the NfERG2 model is shown in Fig. 2b. The high quality of alignment and lack of long insertions or deletions resulted in a low-energy model. The stereochemical quality of the model was checked through Ramachandran plot generated with ProCheck [31]. 82.6% of the residues have Phi and Psi angles in the most favored regions, 16.5% of residues in the allowed regions, and 0.8% of residues in the generously allowed regions (see Fig S1). None of the residues are in the disallowed regions, indicating the overall satisfactory quality. A well-defined 505 $Å^3$ pocket/cavity was identified (Fig. 2b) using ICMPocketFinder utilizing mathematical transformation of the surface attraction fields [25]. The shape and size of the identified pocket are compatible with small molecule inhibitors. The binding pocket residues of NfERG2 are similar to corresponding residues of human σ1 receptor (20% identity and 74% similarity). However, the larger size of the pocket and residue differences may be sufficient to identify NfERG2-specific inhibitors.

Two residues of the binding site, Y163 and E232, are believed to be important for the enzymatic reaction of NfERG2, as they are highly conserved among ERG2 enzymes of different organisms [32]. Furthermore, the predicted binding pose of ERG2 substrate, zymosterol, shows that the negatively charged E232 is in proximity of the C8 carbon of the substrate and may stabilize the transition state carbocation formed at C8 during isomerization reaction. Y163 can form a hydrogen bond with E232 and further stabilize the transition state of substrates by interacting with the carbocation [33]. In addition, mutagenesis experiments and crystal structure confirmed the essentiality of the corresponding residues, Y103 and E172, for the ligand binding to human σ1 receptor [24, 34]. The pocket around those two residues in its lowest energy conformation was used as the binding site for further *in silico* screening of large compound library.

In-silico screening of ERG2 inhibitors

An in-house chemical library at the Center for Discovery and Innovation in Parasitic Diseases (CDIPD) was donated by Biosero Inc. It contains over 26,000 compounds with an average molecular weight of 445±115, cLogP of 4.1±2 and polar surface area (PSA) of 75±33. The library was digitized and pre-filtered for *in silico* screening. Approximately 16,000 compounds with the volume ranging from 400 $Å^3$ to 600 $Å^3$ were docked to the pre-defined binding site of the NfERG2 model. Thirty computationally predicted hits with the highest scores were experimentally tested against proliferating *N. fowleri* trophozoites. The chemical structures of top scoring hits and their docking scores are shown in Fig. 3.

Anti-proliferative activity of compounds in cell-based assay

An *in vitro* assay used to test the anti-proliferative activities of top scoring compounds was developed and validated previously [35]. *N. fowleri* KUL strain in trophozoite form, used in

the assay, is highly pathogenic and causes mortality in mice within seven days, and the strain relevance and applicability was validated previously [16, 18, 36–38]. Thirty compounds were first tested at 50 μM concentration (EC_{50} of miltefosine); eight compounds (highlighted in green in Fig. 3) showed 100% inhibition in this assay and were further evaluated for purity, identity and dose-response. The purity and identity of 8 hits were confirmed by HPLC-MS analysis. Based on LC-MS peak area in the total ion current (TIC) chromatograms, the purity of all compounds was >98%, except for compound 7 which was >95% pure (see Fig S3–S10 in supplementary data). The half- maximal effective concentrations (EC_{50}) for *N. fowleri* proliferation were estimated using Prism 7.0.1. Fig. 4 shows the dose-response curves (blue) for all eight active compounds along with the observed EC_{50} values ranging from 6.4 μM to 25.8 μM. The compounds 23 and 25 were observed to be most potent among 8 active compounds. The observed EC_{50} values for the compounds 23 and 25 were 8.2 μM (95% CI: 4.6 – 15.5) and 6.4 μM (95% CI: 4.3 – 9.2), respectively. The compounds 5, 19 and 28 showed approximately the same EC_{50} values of 11.1 μM (95% CI: 10.1 – 12.6), 11.4 μM (95% CI: 11.3 – 11.5) and 11.2 μM (95% CI: 6.5 – 15.2), respectively. However, the compound 7 and 15 were less potent in inhibiting *N. fowleri* proliferation and had EC_{50} of 20.8 μM (95% CI: 18.9 – 22.8) and 25.8 μM (95% CI: 17.0 – 31.3), respectively in this assay. Activities of these compounds against the cyst stage of *N. fowleri* were not evaluated, since, according to the CDC, cysts are not found in the brain, and are unlikely to be involved in the acute phase of the disease in human [9].

Cytotoxicity assay in HEK-293 cells

To address cytotoxicity of the eight validated compounds, we performed a cell viability assay using HEK-293 cells at serially diluted concentrations of eight active compounds, with a highest concentration of 100 μM. The half-maximal lethal concentrations (LC_{50}s) were estimated from the concentration-response curves (shown as red in Fig. 4). The cell viability was assessed after 72-hour incubation of different concentrations of test compounds with HEK-293 cells. Cell viability was determined using Alamar Blue assay [39]. The compounds 7, 15, 25 and 30 were cytotoxic to HEK293 cells, with LC_{50} values of 42.1, 37.1, 44 and 24.8 μM, respectively (95% CI in Table 1). Whereas, the compounds 5, 19, 23 and 28 have not showed cytotoxicity at amoebicidal concentrations and did not kill HEK293 cells at concentrations higher than 50 μM (observed LC_{50} more than 100 μM).

Selectivity index (SI) was calculated as the ratio of observed LC_{50} (for HEK293 cells) to EC_{50} (for *N. fowleri* cells). A compound with SI of 10 or more is considered selective according to Quispe and collaborators [40]. Compounds 5, 19, 23 and 28 had a selectivity index (SI) greater than 10 showing low or no cytotoxicity to mammalian HEK-293 cells. These four compounds with strong amoebicidal properties and low human cell toxicities fall into two distinct and novel chemical scaffolds with drug like properties.

Analysis of the docking poses of eight experimentally active compounds

The optimal binding poses of all eight compounds were well-defined and are consistent with the asymmetric shape of the binding pocket. All eight compounds (represented as yellow sticks in Fig. 5) showed good space and surface property fits in NfERG2 binding cavity (presented as red mesh). The detailed ligand-target interactions are shown in the

supplementary figure S11 – S18 as 2D interaction diagrams. In all predicted binding poses, residues Y163 and E232 are involved in the ligand-target interactions, which is consistent with the conserved nature of these residues in the ERG2 protein family (Fig. 2a). In addition to residues Y163 and E232, the docked compounds also form hydrogen bonds with N144, C146, and/or Y167 of NfERG2, which confers the polar group complementarity.

Brain permeability assessment of active compounds

To be active against *N. fowleri* residing in the CNS, the drugs must be able to cross the blood-brain barrier (BBB). To analyze the BBB permeability properties of the active compounds, we calculated the BBB permeability multi-parameter score (abbreviated as BBB-MPO) for each compound based on five physicochemical parameters (calculated partition coefficient cLogP, molecular weight MW, topological polar surface area PSA, number of hydrogen bond donors HBD, and pKa of the most basic center). The calculated physicochemical parameters used to estimate the BBB-MPO scores of the active compounds are shown in Supplementary Fig S2.

The range of BBB-MPO score, originally introduced by Pfizer scientists in 2010 [41–42], is from zero to five, and the majority of known BBB permeable drugs have BBB-MPO scores higher than or equal to 3. Four compounds 5, 23, 25 and 28 (out of eight active compounds) have shown BBB-MPO scores greater than 3, indicating their potential for BBB permeability (Table 1). Compound 19 showed a calculated BBB-MPO score of 2.97, which is very close to 3, and is likely to cross BBB to some extent. For the other three compounds, further modifications may be needed to increase their BBB permeability. Furthermore, the compounds with desired BBB-MPO scores also had lower EC_{50} values in the cell-based assay, making them promising candidates for further evaluation and development.

Sterol biosynthesis is a basic metabolic pathway of eukaryotes giving rise to essential membrane components. For the purpose of drug discovery, it offers an array of druggable molecular targets accessible for homology modeling and structure-based screening. Targeting sterol Δ8–Δ7-isomerase (ERG2) in *N. fowleri*, an enzyme without an ortholog in human proteome, opens up a possibility of identifying novel drug candidates for the treatment of PAM [16, 18]. Emopamil-binding protein (EBP), a functional counterpart of ERG2 in humans, shares no sequence similarity with ERG2 (Fig. S19). Recently released crystal structure of human EBP (PDB IDs: 6OHT, 6OHU) is topologically different from ERG2 [33]. While no ERG2 enzymes from any species have been characterized crystallographically, we found a receptor with sufficient sequence similarity and 2.5Å-resolution structure. Based on the structural similarity between the catalytic domain of ERG2 and the human σ_1 non-opioid receptor, we built a homology model for NfERG2. This model was sufficient to identify novel inhibitory scaffolds with good efficacy.

The predictive power of the computational methods depends on the reliability of the model used for *in silico* screening. Even though the sequence identity between the template and NfERG2 was moderate, the chosen strategy worked well due to the strong conservation of the backbone topology evidenced by lack of the insertions or deletions in the protein scaffold around the binding pocket. A relatively high hit rate (8 active hits out of 30 experimentally tested predictions) further implies reasonably good conformation accuracy of

the binding pocket. The EC_{50} of these eight hits was confirmed to be in a low micromolar range. As an added bonus, four compounds had selectivity index greater than 10 against human HEK-293 cells and high blood-brain barrier permeability scores.

The top four validated compounds fall into two novel chemical scaffolds. Compound 5 and 23 both contain a fluorene moiety which fits well into the binding pocket and also contains a nucleophilic carbon in the center feasible for further chemical modifications. Compound 19 and 28 share the same piperidine-spirohydantoin core that doesn't exist in approved drugs, and have two different attachments that can be modified to optimize the efficacy, specificity, or ADMET properties.

The results also emphasize that homology modeling of essential targets in rare pathogen (followed by docking screen of a large chemical library and experimental testing of top hits) is a useful initial strategy even in absence of crystal structures of those targets [43–44]. The chemical diversity of identified hits is a further evidence of this approach.

As far as target specificity is concerned, it is most likely that the identified compounds are not uniquely specific to NfERG2. The ergosterol biosynthesis pathway includes multiple reaction steps catalyzed by different enzymes utilizing structurally similar substrates. It is quite common for compounds to act on more than one enzyme in the sterol biosynthetic pathway [16, 45]. Further studies are needed to characterize the full profile of affected molecular targets responsible for the amoebicidal mechanism of identified hits.

Conclusion

In summary, the four identified new amoebicidal candidates with low HEK-293 cell toxicities and acceptable brain permeability scores fall into two different and novel scaffolds. They were identified through target-based screen using a homology model followed by experimental screen of only 30 compounds and the validation of the top eight candidates. The next steps would include compound optimization, formulation and testing in an animal model of PAM, either alone or in combination with other treatments.

Methods and Materials

Software

Sequence alignment, homology modeling of ERG2, pocket identification and virtual ligand screening were performed using the inbuilt tools of ICM-Pro (version v3.8–6a)[30].

Sequence alignment of ERG2 in various organisms

369 ERG2 sequences from different organisms were downloaded from UniProt via searching "C-8 sterol isomerase" in the protein name field, including ERG2 of *N. fowleri*. Sequence alignment was generated using ICM-Pro using the zero end-gap global alignment method [32]. The comparison matrix was introduced by Gonnet et. al. [46]. A residue conservation profile was generated to show the amino acids essential for the structure and function of the protein. The amino acid counts were normalized by the same factor (1/369) in all alignment positions.

Homology modeling of ERG2 of *N. fowleri*

The crystal structure of the human σ1 receptor (PDB ID: 5HK1) was used as a template. Sequence alignment of ERG2 of *N. fowleri* and human σ1 receptor for homology modeling was built through the zero end-gap global alignment method with the Gonnet comparison matrix [46–47]. The gap opening and extension penalty were set as 2.4 and 0.15, respectively. A pP value was calculated to show the probability that the alignment was random, shown as equation 1. Based on the alignment and structure template, homology model of ERG2 of *N. fowleri* was built with the default parameters in ICM-Pro, with all side chains and insertions/deletions sampled and refined via a biased probability Monte Carlo method[48].

$$pP = -\log_{10}(P\,value) \quad \text{equation (1)}$$

Tentative pocket identification and potential maps generation

In the homology model of ERG2 of *N. fowleri,* a tentative pocket was identified using the ICMPocketFinder tool of ICM-Pro [25], with default values of input parameter (tolerance = 4.6). The calculated volume of the predicted pocket was used to pre-filter compounds for docking with a 20% margin. Based on the identified pocket, the docking region was defined. The potential maps for the docking screen were calculated on a 0.5 Å 3D grid, containing: (i) van der Waals interactions; (ii) electrostatic interactions; (iii) hydrogen bonds; and (iv) hydrophobic potentials.

Virtual ligand screening for *N. fowleri* inhibitors

Virtual ligand screening was conducted by docking a digitized in-house chemical diversity library of the Center for Discovery and Innovation in Parasitic Diseases (CDIPD) containing over 26,000 small molecules to the pre-defined pocket on ERG2 of *N. fowleri* and ranking them by docking scores. Prior to the docking screen, chemicals in the library were filtered by their volumes to fit the predicted pocket volume with a 20% margin. The docking and scoring of each chemical was conducted using a stochastic global energy optimization procedure in internal coordinates [49] implemented in the ICM-Pro v3.8–6a, described as the following steps. 1) A ligand was sampled in an implicit solvent model to generate a series of starting conformations, and each starting conformation was placed into the binding pocket with four principal orientations. 2) The ligand was sampled in the pre-calculated potential maps through biased probability Monte Carlo sampling to optimize the position and internal variables of the ligand. 3) For each ligand, 10 top ranking conformations were optimized and re-scored with ICM full atom scoring function [50], and conformations with the best docking score were kept for comparison. 4) All filtered chemicals were docked to the selected pocket on ERG2 of *N. fowleri* following the above procedures with a computing cluster containing 128 cores. After docking, all chemicals were ranked by their docking scores and the top 30 hits were tested experimentally [51].

Blood-brain barrier permeability score calculation

The BBB permeability scores were evaluated by the BBB-MPO method for the eight active compounds. The BBB-MPO score is calculated by transforming five physicochemical

properties of a compound, calculated partition coefficient (CLogP), molecular weight (MW), topological polar surface area (PSA), number of hydrogen bond donors (HBD), and pKa of the most basic center into a number ranging from zero to five. Detailed description of BBB-MPO score calculation can be found in the ICM manual and the original publications [30, 41–42].

Chemicals and reagents

White, solid flat-bottom 96-well microplates (GREINER BIO-ONE). A CellTiter-Glo luminescence-based cell viability assay kit (Promega Corporation). Dimethyl Sulfoxide (DMSO) and amphotericin B, both purchased from Sigma-Aldrich. The 30 compounds selected for *in vitro* testing were taken from an in-house chemical diversity library of the CDIPD containing over 26,000 compounds (average molecular weight of 445±115, CLogP of 4.1±2 and PSA of 75±33) donated by Biosero Inc. Each compound was prepared as a 10 mM DMSO solution.

Proliferation Inhibition assay for N. fowleri

N. fowleri strain KUL, originally isolated from human cerebrospinal fluid in Belgium in 1973 [52], was obtained from ATCC. KUL is type 3 strain based on the length of the internal transcribed spacers 1 (ITS1), with the T at position 31 in the 5.8S rDNA sequence [2]. The trophozoites were cultured axenically in Nelson medium and 10% fetal bovine serum at 37°C. All experiments were performed using cells harvested during the logarithmic phase of growth. All experiments were conducted in a biosafety cabinet following the BSL-2 procedures as specified in the UCSD Biosafety Practice Guidelines.

Primary screening: negative control wells in the screening plates contained 0.5% DMSO, and positive-control wells contained 50 μM amphotericin B (Sigma-Aldrich). The assay was performed in triplicate. *N. fowleri* trophozoites (10,000 amebae per well) were plated in 96-well plates with Nelson medium. The test compounds (diluted in Nelson medium) were added to the wells to achieve a final concentration of 50 μM in each well. Total volume in each well was 100 μL. Assay plates were incubated for 48 hours at 37°C.

Secondary screen for potency determination: For confirmatory screens of the best hits from the primary screen, serial dilutions of test compounds were prepared from 10 mM stock. For determination of half-maximal effective concentration (EC_{50}), the stocks (10 mM) were diluted with DMSO to yield a 2X serial dilution with a concentration range of 0.39–50 μM. The serially diluted compounds were added to the wells of 96-well plates and *N. fowleri* trophozoits (10,000 amebae per well) were added in each well. The assays were performed in triplicate. Assay plates were incubated at 37°C for 48 hours.

Estimation of bioluminescence: At the end of incubation period, 50 μL of Cell Titer-Glo luminescent cell viability reagent was added to each well of the plate. The plates were then placed on an orbital shaker at room temperature for 10 min to induce cell lysis. After lysis, the plates were equilibrated at room temperature for 10 min to stabilize the luminescent signal. The resulting ATP bioluminescence was measured at room temperature by use of a Perkin Elmer Envision plate reader. Data were expressed as mean ± standard deviation for all experiments. The results were analyzed using a non-linear regression in Prism 7.0.1.

Cell toxicity assay

HEK293 cells (ATCC) were cultured in DMEM+10% FBS culture media in tissue culture treated (Corning, 430641U) flasks at 37 °C, 5% CO_2. The cells were plated at 5000 cells per well in 90 μL of respective media in tissue culture treated (Falcon, 353219) 96-well plates. 10 μL of test compound dilution prepared in culture media was added at different serially diluted concentrations (100 μM and lower) and incubated the plate for at least 72 hours at 37 °C. After the incubation period, 8 μL of Alamar blue dye (Invitrogen, DAL1100) was added to each well, the cells were incubated for 2–4 hours, and then analyzed using SpectraMax fluorescence reader using excitation and emission wavelengths of 544 nm and 590 nm, respectively. Data were expressed as mean ± standard error of mean for all experiments. The results were analyzed using a non-linear regression in Prism 7.0.1.

HPLC-MS/MS analysis

The purity and identity of eight active compounds was confirmed by the HPLC-MS/MS method with the following steps. The compound stock solutions (DMSO at 10 mM) were dissolved in HPLC-MS grade methanol to obtain a concentration of 0.05 mg/mL. These samples were analyzed with an ultra-high-performance liquid chromatography device (Vanquish, Thermo Scientific) coupled to a quadrupole-Orbitrap mass spectrometer (Q Exactive, Thermo Scientific). Chromatographic separation was done using a Kinetex C18 1.7 μm (Phenomenex, Torrance, USA), 100 Å pore size, 2.1 mm (internal diameter) × 150 mm (length) column with a C18 guard cartridge (Phenomenex). The column was maintained at 40°C. The mobile phases used were 0.1% formic acid in water (A) and 0.1% formic acid in acetonitrile (B), and the flow rate was set to 0.5 mL/min. Chromatographic elution gradient was: 0.00–1.00 min, 5% B; 1.00 – 15.00 min, 5% to 100% B; 15.00 −16.9 min, 100% B; 17.0 – 19.0 min, 5% B. The injection volume was set to 1 μL.

Mass spectrometry experiments were performed in electrospray ionization, operating in positive ionization mode with a heated electrospray ionization source. The following source parameters were used: spray voltage, +3000 V; heater temperature, 370°C; capillary temperature, 350°C; S-lens RF, 55 (arb. units); sheath gas flow rate, 55 (arb. units); and auxiliary gas flow rate, 20 (arb. units). The MS^1 scans were acquired at a resolution of 35,000 (at m/z 200) for the 100–1500 m/z range, and the MS^2 scans at a resolution of 17,500 from 0.48 to 16.0 min. The automatic gain control (AGC) target and maximum injection time were set at 5×10^5 and 150 ms for MS1 and MS^2 scans. Up to four MS^2 scans in the data-dependent mode were acquired for most abundant ions per duty cycle, with a starting value of m/z 70. Higher-energy collision-induced dissociation was performed with a normalized collision energy of 20, 35, 50 eV. The apex trigger mode was used (2–7 sec) and the isotopes were excluded. The dynamic exclusion parameters were to 6 sec. Compound purity was estimated by integration of the HPLC-MS peak area.

LC-MS/MS data conversion, analysis and deposition

Thermo raw data were converted to m/z extensible markup language (mzML) in centroid mode using MSConvert (part of ProteoWizard) [53]. The data were visualized with the TOPPView OpenMS software [54]. The mass spectrometry data have been deposited on the MassIVE public repository under the accession number MSV000083490. The reference

spectra were deposited to GNPS spectral library (CCMSLIB00004752955 - CCMSLIB00004752981) [55].

Supplementary Material

Refer to Web version on PubMed Central for supplementary material.

Acknowledgements

The authors thank Dr. Jair Lage De Siqueira Neto for providing the CDIPD compound collection. We also thank Ittipat Meewan and Conall Sauvey for manual annotation of the compound collection and proofreading the manuscript. We thank Dr. Pieter Dorrestein and Collaborative Mass Spectrometry Innovation Center for providing access to the LC-MS facilities and expertise to validate the chemical identities of the hit compounds. This work was partially supported by the UCSD Academic Senate bridge fund program to RA, grants 1KL2TR001444 and R21AI133394 from NIH to AD.

Abbreviations

BBB	blood-brain barrier
CNS	central nervous system
MPO	multi-parameter optimization
PAM	primary amoebic meningoencephalitis
SI	selectivity index
CI	confidence interval

References

1. Yoder JS; Eddy BA; Visvesvara GS; Capewell L; Beach MJ, The epidemiology of primary amoebic meningoencephalitis in the USA, 1962–2008. Epidemiology and Infection 2009, 138 (7), 968–975. DOI: 10.1017/S0950268809991014. [PubMed: 19845995]
2. De Jonckheere JF, Origin and evolution of the worldwide distributed pathogenic amoeboflagellate Naegleria fowleri. Infection, Genetics and Evolution 2011, 11 (7), 1520–1528. DOI: 10.1016/j.meegid.2011.07.023.
3. Siddiqui R; Ali IKM; Cope JR; Khan NA, Biology and pathogenesis of Naegleria fowleri. Acta Tropica 2016, 164 375–394. DOI: 10.1016/j.actatropica.2016.09.009. [PubMed: 27616699]
4. Javanmard E; Niyyati M; Lorenzo-Morales J; Lasjerdi Z; Behniafar H; Mirjalali H, Molecular identification of waterborne free living amoebae (Acanthamoeba, Naegleria and Vermamoeba) isolated from municipal drinking water and environmental sources, Semnan province, north half of Iran. Experimental Parasitology 2017, 183, 240–244. DOI: 10.1016/j.exppara.2017.09.016. [PubMed: 28916458]
5. Reyes-Batlle M; Wagner C; López-Arencibia A; Sifaoui I; Martínez-Carretero E; Valladares B; Piñero Jose E; Lorenzo-Morales J, Isolation and molecular characterization of a Naegleria strain from a recreational water fountain in Tenerife, Canary Islands, Spain. In Acta Parasitologica, 2017; Vol. 62, p 265 DOI: 10.1515/ap-2017-0033. [PubMed: 28426408]
6. John DT, Primary Amebic Meningoencephalitis and the Biology of Naegleria fowleri. Annu. Rev. Microbiol. 1982, 36 (1), 101–123. DOI: 10.1146/annurev.mi.36.100182.000533. [PubMed: 6756287]
7. Cervantes-Sandoval I; Serrano-Luna J. d. J.; Meza-Cervantez P; Arroyo R; Tsutsumi V; Shibayama M, Naegleria fowleri induces MUC5AC and pro-inflammatory cytokines in human epithelial cells

via ROS production and EGFR activation. Microbiology 2009, 155 (11), 3739–3747. DOI: doi:10.1099/mic.0.030635-0. [PubMed: 19661176]

8. Cervantes-Sandoval I; Serrano-Luna J. d. J.; García-Latorre E; Tsutsumi V; Shibayama M, Characterization of brain inflammation during primary amoebic meningoencephalitis. Parasitology International 2008, 57 (3), 307–313. DOI: 10.1016/j.parint.2008.01.006. [PubMed: 18374627]
9. Naegleria fowleri — Primary Amebic Meningoencephalitis (PAM) — Amebic Encephalitis. https://www.cdc.gov/parasites/naegleria/index.html (accessed December 10th).
10. Linam WM; Ahmed M; Cope JR; Chu C; Visvesvara GS; da Silva AJ; Qvarnstrom Y; Green J, Successful Treatment of an Adolescent With Naegleria fowleri Primary Amebic Meningoencephalitis. Pediatrics 2015, 135 (3), e744 DOI: 10.1542/peds.2014-2292. [PubMed: 25667249]
11. Cope JR; Conrad DA; Cohen N; Cotilla M; DaSilva A; Jackson J; Visvesvara GS, Use of the Novel Therapeutic Agent Miltefosine for the Treatment of Primary Amebic Meningoencephalitis: Report of 1 Fatal and 1 Surviving Case. Clinical Infectious Diseases 2015, 62 (6), 774–776. DOI: 10.1093/cid/civ1021. [PubMed: 26679626]
12. Seidel JS; Harmatz P; Visvesvara GS; Cohen A; Edwards J; Turner J, Successful Treatment of Primary Amebic Meningoencephalitis. N. Engl. J. Med. 1982, 306 (6), 346–348. DOI: 10.1056/NEJM198202113060607. [PubMed: 7054710]
13. Mesa-Arango AC; Scorzoni L; Zaragoza O, It only takes one to do many jobs: Amphotericin B as antifungal and immunomodulatory drug. Frontiers in Microbiology 2012, 3 (286). DOI: 10.3389/fmicb.2012.00286.
14. Baginski M; Czub J, Amphotericin B and Its New Derivatives – Mode of Action. Current Drug Metabolism 2009, 10 (5), 459–469. DOI: 10.2174/138920009788898019. [PubMed: 19689243]
15. Ghannoum MA; Rice LB, Antifungal agents: mode of action, mechanisms of resistance, and correlation of these mechanisms with bacterial resistance. Clinical microbiology reviews 1999, 12 (4), 501–517. DOI: 10.1128/CMR.12.4.501. [PubMed: 10515900]
16. Debnath A; Calvet CM; Jennings G; Zhou W; Aksenov A; Luth MR; Abagyan R; Nes WD; McKerrow JH; Podust LM, CYP51 is an essential drug target for the treatment of primary amoebic meningoencephalitis (PAM). PLoS neglected tropical diseases 2017, 11 (12), e0006104 DOI: 10.1371/journal.pntd.0006104. [PubMed: 29284029]
17. Schuster FL; Guglielmo BJ; Visvesvara GS, In-Vitro Activity of Miltefosine and Voriconazole on Clinical Isolates of Free-Living Amebas: Balamuthia mandrillaris, Acanthamoeba spp., and Naegleria fowleri. Journal of Eukaryotic Microbiology 2006, 53 (2), 121–126. DOI: 10.1111/j.1550-7408.2005.00082.x. [PubMed: 16579814]
18. Zhou W; Debnath A; Jennings G; Hahn HJ; Vanderloop BH; Chaudhuri M; Nes WD; Podust LM, Enzymatic chokepoints and synergistic drug targets in the sterol biosynthesis pathway of Naegleria fowleri. PLOS Pathogens 2018, 14 (9), e1007245 DOI: 10.1371/journal.ppat.1007245. [PubMed: 30212566]
19. Kethireddy S; Andes D, CNS pharmacokinetics of antifungal agents. Expert Opinion on Drug Metabolism & Toxicology 2007, 3 (4), 573–581. DOI: 10.1517/17425255.3.4.573. [PubMed: 17696807]
20. Raederstorff D; Rohmer M, The Action of the Systemic Fungicides Tridemorph and Fenpropimorph on Sterol Biosynthesis by the Soil Amoeba Acanthamoeba Polyphaga. Eur. J. Biochem. 1987, 164 (2), 421–426. DOI: 10.1111/j.1432-1033.1987.tb11074.x. [PubMed: 3569273]
21. Nes Craigen R.; Singha Ujjal K.; Liu J; Ganapathy K; Villalta F; Waterman Michael R.; Lepesheva Galina I.; Chaudhuri M; Nes WD, Novel sterol metabolic network of Trypanosoma brucei procyclic and bloodstream forms. Biochemical Journal 2012, 443 (1), 267 DOI: 10.1042/BJ20111849. [PubMed: 22176028]
22. Zhou W; Warrilow AGS; Thomas CD; Ramos E; Parker JE; Price CL; Vanderloop BH; Fisher PM; Loftis MD; Kelly DE; Kelly SL; Nes WD, Functional importance for developmental regulation of sterol biosynthesis in Acanthamoeba castellanii. Biochimica et Biophysica Acta (BBA) - Molecular and Cell Biology of Lipids 2018, 1863 (10), 1164–1178. DOI: 10.1016/j.bbalip.2018.07.004. [PubMed: 30044954]

23. Choi JY; Podust LM; Roush WR, Drug Strategies Targeting CYP51 in Neglected Tropical Diseases. Chemical Reviews 2014, 114 (22), 11242–11271. DOI: 10.1021/cr5003134. [PubMed: 25337991]
24. Schmidt HR; Zheng S; Gurpinar E; Koehl A; Manglik A; Kruse AC, Crystal structure of the human σ1 receptor. Nature 2016, 532, 527 DOI: 10.1038/nature17391. [PubMed: 27042935]
25. An J; Totrov M; Abagyan R, Pocketome via Comprehensive Identification and Classification of Ligand Binding Envelopes. Molecular & Cellular Proteomics 2005, 4 (6), 752–761. DOI: 10.1074/mcp.M400159-MCP200. [PubMed: 15757999]
26. Maurice T; Su T-P, The pharmacology of sigma-1 receptors. Pharmacology & therapeutics 2009, 124 (2), 195–206. DOI: 10.1016/j.pharmthera.2009.07.001. [PubMed: 19619582]
27. Hanner M; Moebius FF; Flandorfer A; Knaus HG; Striessnig J; Kempner E; Glossmann H, Purification, molecular cloning, and expression of the mammalian sigma1-binding site. Proceedings of the National Academy of Sciences 1996, 93 (15), 8072 DOI: 10.1073/pnas.93.15.8072.
28. Moebius FF; Reiter RJ; Hanner M; Glossmann H, High affinity of sigma1-binding sites for sterol isomerization inhibitors: evidence for a pharmacological relationship with the yeast sterol C8–C7 isomerase. British journal of pharmacology 1997, 121 (1), 1–6. DOI: 10.1038/sj.bjp.0701079. [PubMed: 9146879]
29. Moebius FF; Bermoser K; Reiter RJ; Hanner M; Glossmann H, Yeast Sterol C8−C7 Isomerase: Identification and Characterization of a High-Affinity Binding Site for Enzyme Inhibitors. Biochemistry 1996, 35 (51), 16871–16878. DOI: 10.1021/bi961996m. [PubMed: 8988026]
30. Abagyan R; Raush E; Totrov M; Orry A, ICM Manual v3.8–6; Molsoft LCC: San Diego, CA 2017.
31. Laskowski RA; MacArthur MW; Moss DS; Thornton JM, Procheck: A Program to Check the Stereochemical Quality of Protein Structures. J. Appl. Crystallogr. 1993, 26 (2), 283–291. DOI: 10.1107/S0021889892009944.
32. Shi D; Abagyan R; Svetlov D; Artsimovitch I, Flipping states: a few key residues decide the winning conformation of the only universally conserved transcription factor. Nucleic Acids Research 2017, 45 (15), 8835–8843. DOI: 10.1093/nar/gkx523. [PubMed: 28605514]
33. Long T; Hassan A; Thompson BM; McDonald JG; Wang J; Li X, Structural basis for human sterol isomerase in cholesterol biosynthesis and multidrug recognition. Nature Communications 2019, 10 (1), 2452 DOI: 10.1038/s41467-019-10279-w.
34. Seth P; Ganapathy ME; Conway SJ; Bridges CD; Smith SB; Casellas P; Ganapathy V, Expression pattern of the type 1 sigma receptor in the brain and identity of critical anionic amino acid residues in the ligand-binding domain of the receptor. Biochimica et Biophysica Acta (BBA) - Molecular Cell Research 2001, 1540 (1), 59–67. DOI: 10.1016/S0167-4889(01)00117-3. [PubMed: 11476895]
35. Debnath A; Tunac JB; Galindo-Gómez S; Silva-Olivares A; Shibayama M; McKerrow JH, Corifungin, a New Drug Lead against Naegleria, Identified from a High-Throughput Screen. Antimicrobial Agents and Chemotherapy 2012, 56 (11), 5450–5457. DOI: 10.1128/aac.00643-12. [PubMed: 22869574]
36. Debnath A; Nelson AT; Silva-Olivares A; Shibayama M; Siegel D; McKerrow JH, In Vitro Efficacy of Ebselen and BAY 11–7082 Against Naegleria fowleri. Frontiers in Microbiology 2018, 9, 414. [PubMed: 29559968]
37. Zyserman I; Mondal D; Sarabia F; McKerrow JH; Roush WR; Debnath A, Identification of cysteine protease inhibitors as new drug leads against Naegleria fowleri. Experimental Parasitology 2018, 188, 36–41. DOI: 10.1016/j.exppara.2018.03.010. [PubMed: 29551628]
38. Singh A; Nisha; Bains T; Hahn HJ; Liu N; Tam C; Cheng LW; Kim J; Debnath A; Land KM; Kumar V, Design, synthesis and preliminary antimicrobial evaluation of N-alkyl chain-tethered C-5 functionalized bis-isatins. MedChemComm 2017, 8 (10), 1982–1992. DOI: 10.1039/C7MD00434F. [PubMed: 29449910]
39. O'Brien J; Wilson I; Orton T; Pognan F, Investigation of the Alamar Blue (resazurin) fluorescent dye for the assessment of mammalian cell cytotoxicity. European Journal of Biochemistry 2000, 267 (17), 5421–5426. DOI: 10.1046/j.1432-1327.2000.01606.x. [PubMed: 10951200]

40. Quispe M A; Zavala C D; Rojas C J; Posso R M; Vaisberg W A, Efecto citotóxico selectivo in vitro de muricin H(acetogenina de Annona muricata) en cultivos celulares de cáncer de pulmón. Revista Peruana de Medicina Experimental y Salud Pública 2006, 23 (4), 265–269.
41. Wager TT; Hou X; Verhoest PR; Villalobos A, Moving beyond Rules: The Development of a Central Nervous System Multiparameter Optimization (CNS MPO) Approach To Enable Alignment of Druglike Properties. ACS Chemical Neuroscience 2010, 1 (6), 435–449. DOI: 10.1021/cn100008c. [PubMed: 22778837]
42. Wager TT; Hou X; Verhoest PR; Villalobos A, Central Nervous System Multiparameter Optimization Desirability: Application in Drug Discovery. ACS Chemical Neuroscience 2016, 7 (6), 767–775. DOI: 10.1021/acschemneuro.6b00029. [PubMed: 26991242]
43. Zhong H-J; Wang W; Kang T-S; Yan H; Yang Y; Xu L; Wang Y; Ma D-L; Leung C-H, A Rhodium(III) Complex as an Inhibitor of Neural Precursor Cell Expressed, Developmentally Down-Regulated 8-Activating Enzyme with in Vivo Activity against Inflammatory Bowel Disease. Journal of Medicinal Chemistry 2017, 60 (1), 497–503. DOI: 10.1021/acs.jmedchem.6b00250. [PubMed: 27976900]
44. Yang C; Wang W; Chen L; Liang J; Lin S; Lee M-Y; Ma D-L; Leung C-H, Discovery of a VHL and HIF1α interaction inhibitor with in vivo angiogenic activity via structure-based virtual screening. Chemical Communications 2016, 52 (87), 12837–12840. DOI: 10.1039/C6CC04938A. [PubMed: 27709157]
45. Yates CM; Garvey EP; Shaver SR; Schotzinger RJ; Hoekstra WJ, Design and optimization of highly-selective, broad spectrum fungal CYP51 inhibitors. Bioorganic & Medicinal Chemistry Letters 2017, 27 (15), 3243–3248. DOI: 10.1016/j.bmcl.2017.06.037. [PubMed: 28651982]
46. Gonnet GH; Cohen MA; Benner SA, Exhaustive Matching of the Entire Protein Sequence Database. Science 1992, 256 (5062), 1443–1445. DOI: 10.1126/science.1604319. [PubMed: 1604319]
47. Abagyan RA; Batalov S, Do aligned sequences share the same fold?11Edited by F. E. Cohen. Journal of Molecular Biology 1997, 273 (1), 355–368. DOI: 10.1006/jmbi.1997.1287. [PubMed: 9367768]
48. Abagyan R; Totrov M, Biased Probability Monte Carlo Conformational Searches and Electrostatic Calculations for Peptides and Proteins. J. Mol. Biol. 1994, 235 (3), 983–1002. DOI: 10.1006/jmbi.1994.1052. [PubMed: 8289329]
49. Abagyan R; Totrov M; Kuznetsov D, Icm—A New Method for Protein Modeling and Design: Applications to Docking and Structure Prediction From the Distorted Native Conformation. J. Comput. Chem. 1994, 15 (5), 488–506. DOI: 10.1002/jcc.540150503.
50. Neves MA; Totrov M; Abagyan R, Docking and scoring with ICM: the benchmarking results and strategies for improvement. J Comput Aided Mol Des 2012, 26 (6), 675–86. DOI: 10.1007/s10822012-9547-0. [PubMed: 22569591]
51. Svetlov D; Shi D; Twentyman J; Nedialkov Y; Rosen DA; Abagyan R; Artsimovitch I, In silico discovery of small molecules that inhibit RfaH recruitment to RNA polymerase. Molecular Microbiology 2018, 110 (1), 128–142. DOI: 10.1111/mmi.14093. [PubMed: 30069925]
52. Dinauer M; Pierre R, Primary Amoebic Meningoencephalitis After Swimming in Stream Water. The Lancet 1973, 302 (7835), 971 DOI: 10.1016/S0140-6736(73)92635-4.
53. Chambers MC; Maclean B; Burke R; Amodei D; Ruderman DL; Neumann S; Gatto L; Fischer B; Pratt B; Egertson J; Hoff K; Kessner D; Tasman N; Shulman N; Frewen B; Baker TA; Brusniak M-Y; Paulse C; Creasy D; Flashner L; Kani K; Moulding C; Seymour SL; Nuwaysir LM; Lefebvre B; Kuhlmann F; Roark J; Rainer P; Detlev S; Hemenway T; Huhmer A; Langridge J; Connolly B; Chadick T; Holly K; Eckels J; Deutsch EW; Moritz RL; Katz JE; Agus DB; MacCoss M; Tabb DL; Mallick P, A cross-platform toolkit for mass spectrometry and proteomics. Nature Biotechnology 2012, 30, 918–920. DOI: 10.1038/nbt.2377.
54. Röst HL; Sachsenberg T; Aiche S; Bielow C; Weisser H; Aicheler F; Andreotti S; Ehrlich H-C; Gutenbrunner P; Kenar E; Liang X; Nahnsen S; Nilse L; Pfeuffer J; Rosenberger G; Rurik M; Schmitt U; Veit J; Walzer M; Wojnar D; Wolski WE; Schilling O; Choudhary JS; Malmström L; Aebersold R; Reinert K; Kohlbacher O, OpenMS: a flexible open-source software platform for mass spectrometry data analysis. Nature Methods 2016, 13, 741–748. DOI: 10.1038/nmeth.3959. [PubMed: 27575624]

55. Wang M; Carver JJ; Phelan VV; Sanchez LM; Garg N; Peng Y; Nguyen DD; Watrous J; Kapono CA; Luzzatto-Knaan T; Porto C; Bouslimani A; Melnik AV; Meehan MJ; Liu W-T; Crüsemann M; Boudreau PD; Esquenazi E; Sandoval-Calderón M; Kersten RD; Pace LA; Quinn RA; Duncan KR; Hsu C-C; Floros DJ; Gavilan RG; Kleigrewe K; Northen T; Dutton RJ; Parrot D; Carlson EE; Aigle B; Michelsen CF; Jelsbak L; Sohlenkamp C; Pevzner P; Edlund A; McLean J; Piel J; Murphy BT; Gerwick L; Liaw C-C; Yang Y-L; Humpf H-U; Maansson M; Keyzers RA; Sims AC; Johnson AR; Sidebottom AM; Sedio BE; Klitgaard A; Larson CB; Boya P CA; Torres-Mendoza D; Gonzalez DJ; Silva DB; Marques LM; Demarque DP; Pociute E; O'Neill EC; Briand E; Helfrich EJN; Granatosky EA; Glukhov E; Ryffel F; Houson H; Mohimani H; Kharbush JJ; Zeng Y; Vorholt JA; Kurita KL; Charusanti P; McPhail KL; Nielsen KF; Vuong L; Elfeki M; Traxler MF; Engene N; Koyama N; Vining OB; Baric R; Silva RR; Mascuch SJ; Tomasi S; Jenkins S; Macherla V; Hoffman T; Agarwal V; Williams PG; Dai J; Neupane R; Gurr J; Rodríguez AMC; Lamsa A; Zhang C; Dorrestein K; Duggan BM; Almaliti J; Allard P-M; Phapale P; Nothias L-F; Alexandrov T; Litaudon M; Wolfender J-L; Kyle JE; Metz TO; Peryea T; Nguyen D-T; VanLeer D; Shinn P; Jadhav A; Müller R; Waters KM; Shi W; Liu X; Zhang L; Knight R; Jensen PR; Palsson BØ; Pogliano K; Linington RG; Gutiérrez M; Lopes NP; Gerwick WH; Moore BS; Dorrestein PC; Bandeira N, Sharing and community curation of mass spectrometry data with Global Natural Products Social Molecular Networking. Nature Biotechnology 2016, 34, 828–837. DOI: 10.1038/nbt.3597.

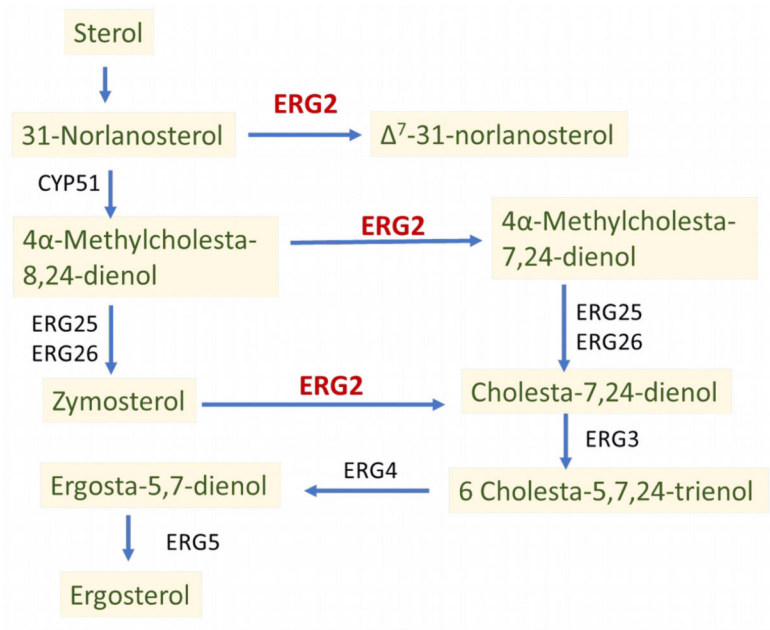

Figure 1. Ergosterol Biosynthesis in *N. fowleri.*

Biosynthetic steps catalyzed by sterol Δ8−Δ7 isomerase (ERG2) in ergosterol biosynthesis in *N. fowleri* as reported elsewhere [18].

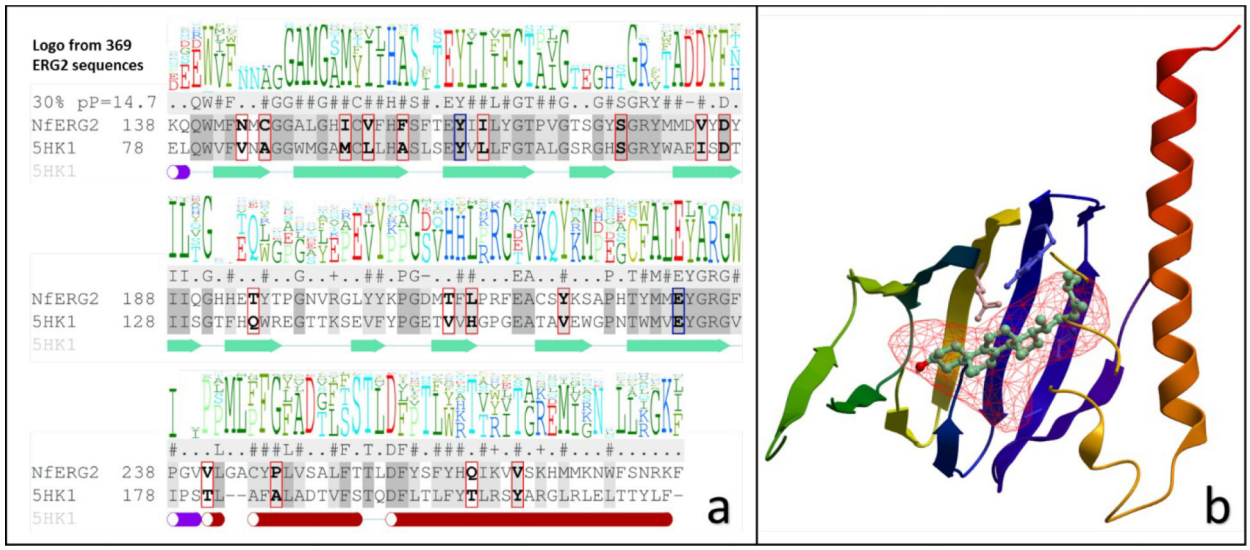

Figure 2. Sequence alignments and homology model of NfERG2.

a) Sequence alignments of NfERG2 and human σ1 receptor ligand binding cavity. Positions with red and blue boxes correspond to residues of the binding pocket in the NfERG2 model. Conservation profile above the NfERG2 sequence was generated from sequence alignment of ERG2 in 369 different organisms. The secondary structure elements of the 5HK1 σ1 receptor are marked by different colors and shapes as following: red cylinder = alpha helix, green arrow = beta sheet, blue cylinder = pi helix, magenta cylinder = 3/10 helix. b) Structure of NfERG2 model in complex with zymosterol. NfERG2 model is colored in rainbow colors to emphasize the N (purple) and C (red) termini. Two residues (Y163 and E232) that are potentially critical for the enzymatic reaction of NfERG2 are shown as stick representations. The red mesh represents the binding pocket of NfERG2. The predicted binding pose of substrate zymosterol in the homology model of NfERG2 is shown in (b).

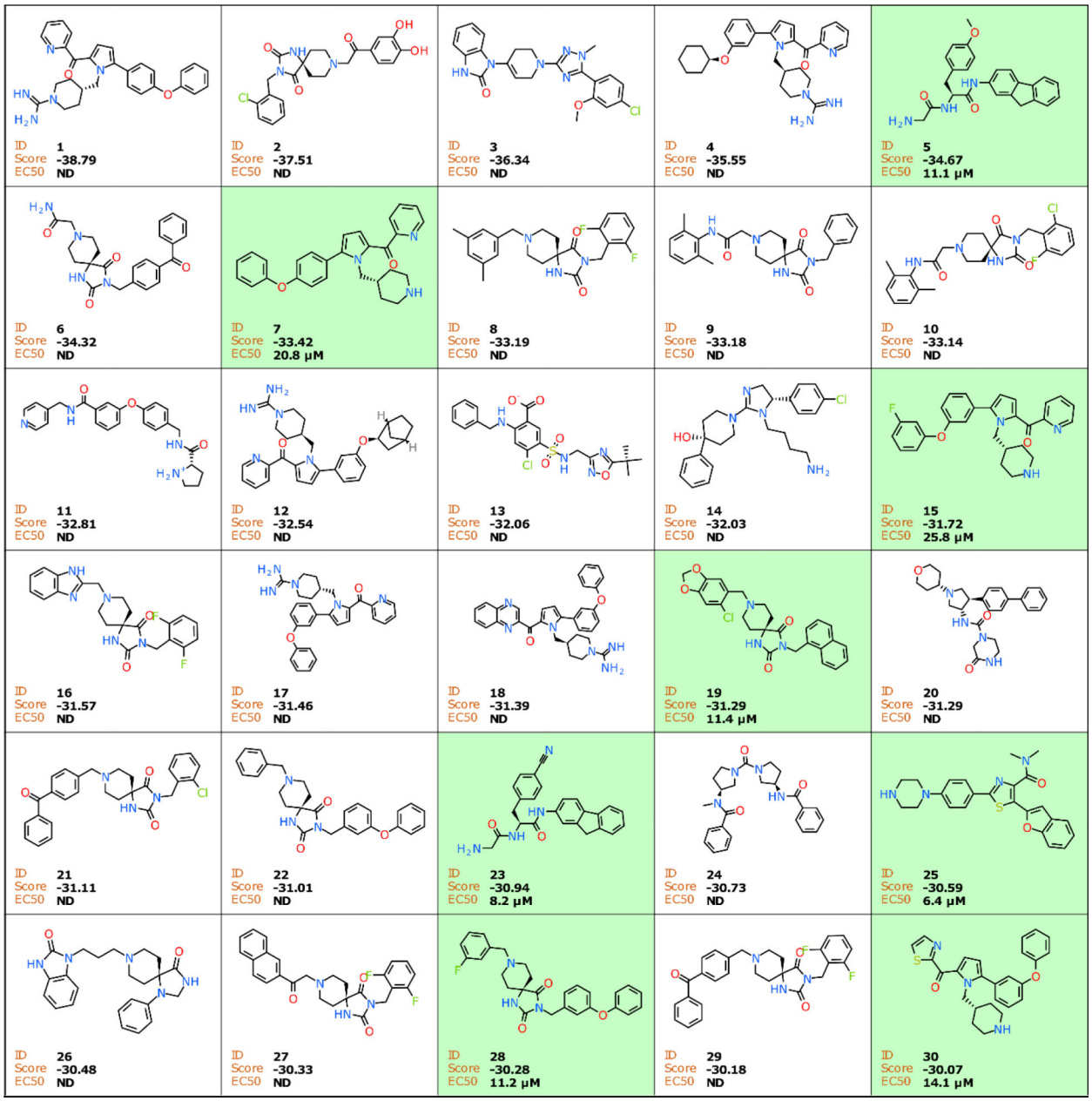

Figure 3. Chemical structures of the top 30 docking hits from the *in-silico* screening.

The compounds are identified by arbitrary numbers as per the docking list generated. Docking score is shown for each chemical structure. All 30 compounds were tested for anti-*N. fowleri* activity in cell-based assay and eight experimentally active compounds are highlighted in green. The EC_{50} values observed for active compounds are also provided with the corresponding structures.

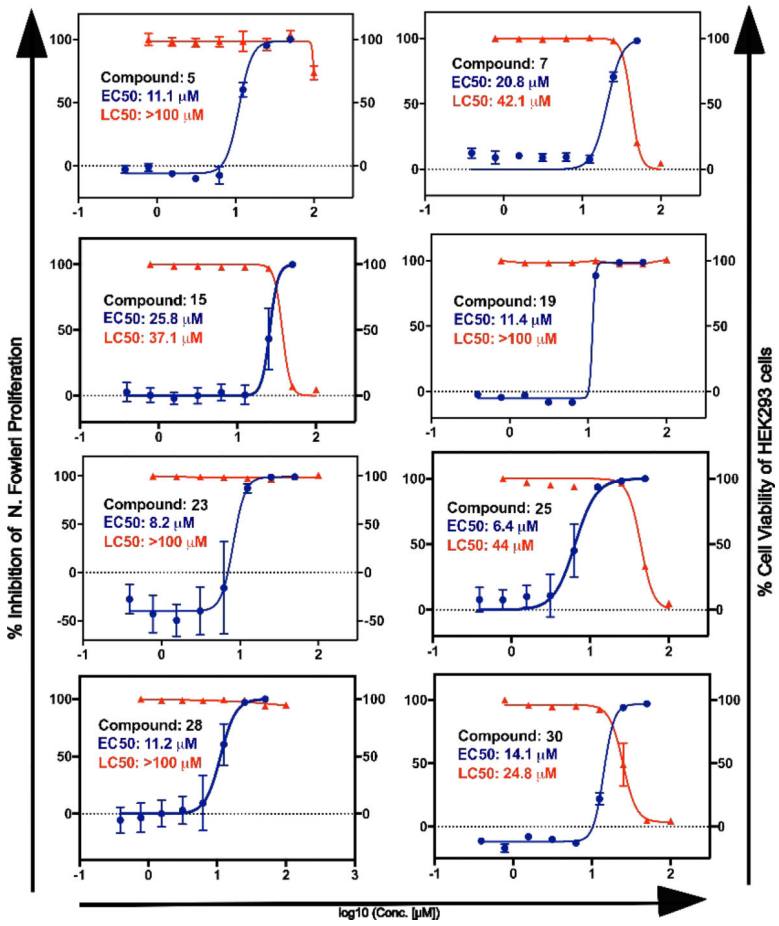

Figure 4. Dose-response curves of active compounds for the *N. fowleri* inhibition (blue) and cell toxicity in human HEK-293 cells (red).

The observed dose-response curve with derived EC_{50} value for *N. fowleri* proliferation inhibition assay, and human cell viability with derived LC_{50} value for HEK293 cell assay are provided for each compound. Image represents the mean and standard error of mean of at least three experiments.

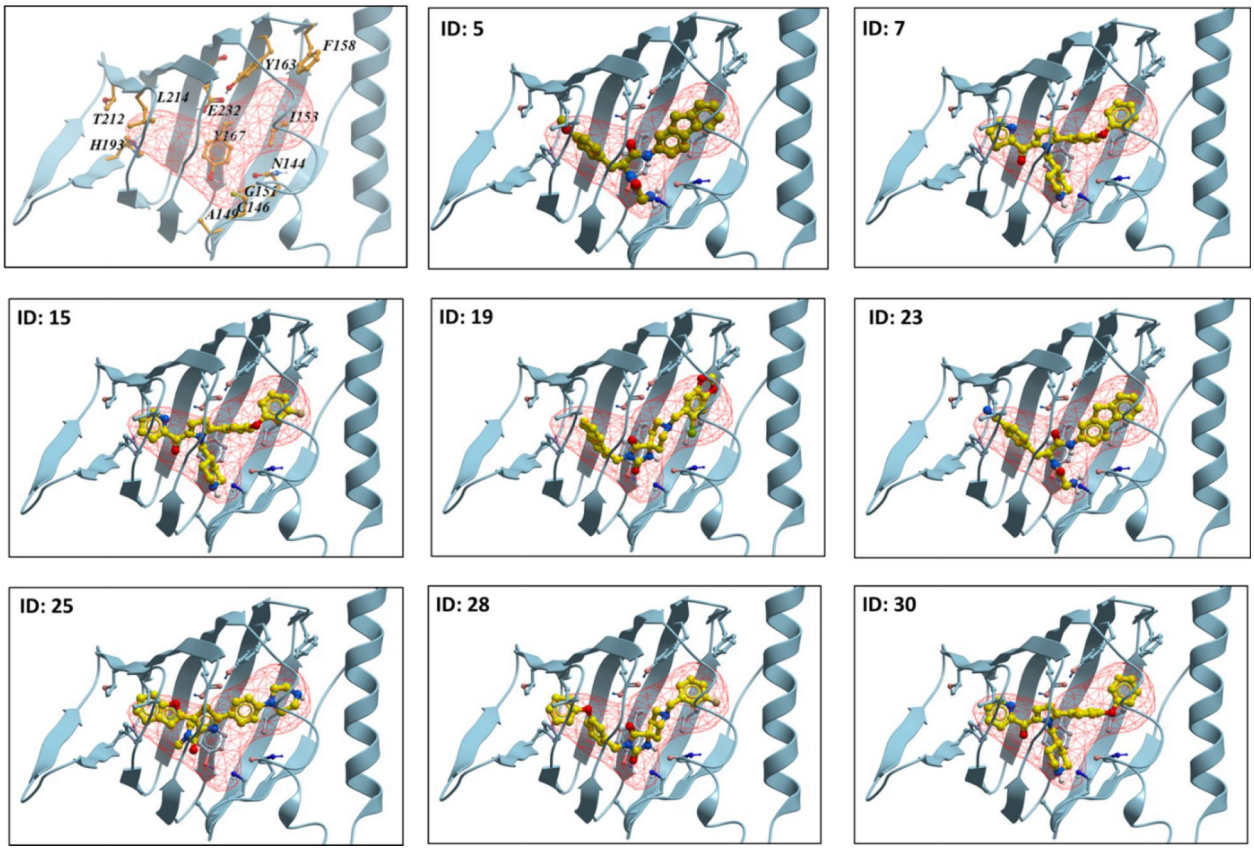

Figure 5. Predicted docking poses of the active compounds in the binding cavity of NfERG2.
NfERG2 is shown as a ribbon, compounds are shown in ball-and-stick mode, and binding pocket of NfERG2 predicted by homology modelling is shown in red mesh.

Table 1.

BBB multi-parameter optimization (BBB-MPO) score of active compounds.

Compounds with BBB-MPO scores >3 are highlighted in blue.

Compound ID	Docking Score	BBB-MPO Score	EC_{50} (μM)	EC_{50} 95% CI	LC_{50} (μM)	LC_{50} 95% CI
5	−34.67	3.85	11.1	10.1 – 12.6	> 100	N.A.
7	−33.42	2.62	20.8	18.9 – 22.8	42.1	40.5 – 43.4
15	−31.72	2.31	25.8	17.0 – 31.3	37.1	36.3 – 37.9
19	−31.29	2.97	11.4	11.3 – 11.5	> 100	N.A.
23	−30.94	3.90	8.2	4.6 – 15.5	> 100	N.A.
25	−30.59	3.68	6.4	4.3 – 9.2	44	47.9 – 48.8
28	−30.28	3.54	11.2	6.5 – 15.2	> 100	N.A.
30	−30.07	2.51	14.1	13 – 15.3	24.8	19.8 – 29.8